

Asymptotic-freedom and massive glueballs in a qubit-regularized SU(2) gauge theory

Rui Xian Siew  ^{1,*} Shailesh Chandrasekharan  ^{1,†} and Tanmoy Bhattacharya  ^{2,‡}

¹*Department of Physics, Box 90305, Duke University, Durham, North Carolina 27708, USA*

²*Theoretical Division, Los Alamos National Laboratory, Los Alamos, New Mexico 87545, USA*

(Dated: January 22, 2026)

We argue that a simple qubit-regularized SU(2) lattice gauge theory (LGT) on a plaquette chain serves as a pseudo-one-dimensional toy model for Yang-Mills (YM) theory in three spatial dimensions. We map the chain Hamiltonian to the Transverse Field Ising Model (TFIM) in a uniform magnetic field and demonstrate that it can be tuned to a continuum limit in which the short-distance physics is governed by the asymptotically free Ising conformal field theory (CFT) describing free Majorana fermions, while the long-distance regime contains massive excitations of the E_8 quantum field theory (QFT) that can be interpreted as one-dimensional analogues of glueballs. Furthermore, we find $\sqrt{\sigma}/m_1 = 0.249(1)$ where σ is the string tension between two static quarks and m_1 is the mass of the lightest glueball.

I. INTRODUCTION

Qubit regularization of QFTs is a framework for recovering a continuum QFT as the limit of low-energy sectors of increasingly large spatial lattices of quantum mechanical systems with a fixed local Hilbert space [1], often describable as a qubit-model. If successful, this approach can provide a way to perform efficient QFT calculations on a quantum computer [2]. The success of this approach is deeply connected to the ideas of universality and renormalization, as originally introduced by Wilson [3]. In particular, it is essential that the qubit-regularized theory possesses a critical point such that, in its vicinity, the long-distance physics is governed by the renormalization group (RG) fixed point corresponding to the desired continuum QFT. This behavior is not guaranteed in general, and an important direction of research is to characterize the critical points of various qubit-regularized theories and to uncover the physics of the fixed points that emerge near them.

Massive QFTs of interest in particle physics typically arise through relevant perturbations of such RG fixed points. These fixed points are characterized as ultraviolet (UV) fixed points, and the associated scale-invariant—often conformally invariant—theories describe the short-distance, or equivalently high-energy, physics of the corresponding massive QFT. Asymptotic freedom of pure non-Abelian gauge theories is a prime example of this feature. A major challenge for the Wilson lattice regularization program is to construct lattice models that exhibit this behavior: i.e., they have a critical point whose long-distance physics is governed by the desired UV fixed point. When a small relevant perturbation is added, the continuum UV physics manifests as an intermediate crossover regime, while the extreme long-distance behavior reproduces the desired massive QFT. A schematic illustration

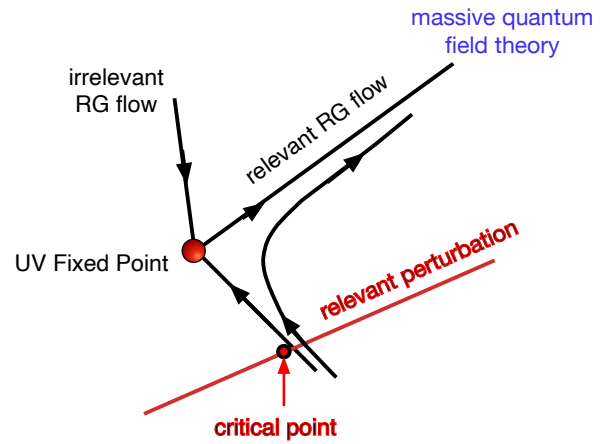


FIG. 1. A schematic illustration of the traditional RG flows in the space of lattice models that reproduce a massive continuum QFT in the IR limit. Typically, one begins with a lattice model tuned to a critical point and then adds a relevant perturbation. The short-distance physics of the resulting massive QFT is governed by the UV fixed point, which can also be viewed as the IR fixed point of the unperturbed lattice model at criticality.

of this traditional RG flow in the space of lattice models is shown in Fig. 1.

In this work, we present an explicit example of such a traditional RG flow realized in a qubit-regularized SU(2) LGT. In our construction, the UV fixed point is described by the two-dimensional Ising-CFT (ICFT), while the corresponding massive theory is the E_8 -QFT (E8QFT) of Zamolodchikov [4].

The qubit-regularized SU(2) LGT considered here is formulated in the Hamiltonian framework on a spatial lattice with the geometry of a plaquette chain. Such a chain is pseudo-one-dimensional in the sense that it is one-dimensional in the thermodynamic limit, but has local gauge ‘plaquette’ excitations. In particular, the physical Hilbert space has scalar adjoint ‘gluons’ at each lattice site that are the remnant of the single transverse gluon

* ruixian.siew@duke.edu

† sch27@duke.edu

‡ tanmoy@lanl.gov

degree of freedom per site in the theory where the ladder is extended to form a genuinely two-dimensional lattice. This view point can be extended to $2 + 1$ dimensions where glue balls arise as weakly coupled system of heavy adjoint particles [5].

Hamiltonian LGTs on plaquette chains have been explored recently in several contexts [6–11]. Here, we extend these investigations by studying relevant perturbations away from critical points where massive continuum QFTs emerge in the IR. In particular, we identify one such critical point in a specific $SU(2)$ gauge theory on a plaquette chain by mapping the chain Hamiltonian to the TFIM in a uniform magnetic field,

$$H = \sum_i (-\sigma_i^z \sigma_{i+1}^z - \sigma_i^x - h\sigma_i^z). \quad (1)$$

It is well known that this Hamiltonian is critical at $h = 0$, where it flows to the ICFT. For small nonzero h , the long-distance physics is instead described by a massive QFT with E_8 symmetry, as predicted by Zamolodchikov [4]. In a qubit-regularized $SU(2)$ LGT, we interpret the massive states as one-dimensional analogues of glueballs. Using the standard step-scaling function, we demonstrate that the continuum theory's short-distance behavior is governed by the ICFT, consistent with the traditional RG flow shown in Fig. 1. Because the ICFT describes free Majorana fermions, we argue that the $SU(2)$ plaquette chain also exhibits asymptotic freedom, much like a three-dimensional YM theory.

II. THE $SU(2)$ PLAQUETTE CHAIN

We recently showed that the physical Hilbert space of $SU(N)$ Hamiltonian LGTs can be constructed efficiently using the monomer-dimer tensor-network (MDTN) basis $|\{\lambda_s\}, \{\lambda_\ell\}, \{\alpha_s\}\rangle$ [11]. Each MDTN basis state is characterized by three sets of labels defined as follows: (i) $\{\lambda_s\}$ denotes the configuration of unitary irreducible representations (irreps) of $SU(N)$ associated with matter fields on the lattice sites, (ii) $\{\lambda_\ell\}$ denotes the configuration of irreps associated with gauge fields on the lattice links, and (iii) $\{\alpha_s\} = 1, 2, \dots, \mathcal{D}(\mathcal{H}_s^g)$ labels the degeneracy of singlet representations in the local site Hilbert space \mathcal{H}_s^g , which is the tensor product of the irreps of the links $\{\lambda_{\ell_s}\}$ connected to the site s and the site representation λ_s .

In this work, we focus on the $SU(2)$ pure gauge theory, which contains no matter fields, allowing us to set all

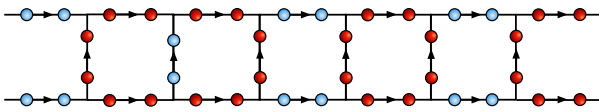


FIG. 2. A pictorial representation of an MDTN basis state in the plaquette chain with $SU(2)$ gauge fields. The blue dots represent $\lambda = 1$ (singlets) and the red dots represent $\lambda = 2$ (doublets).

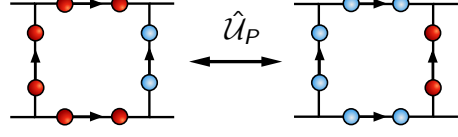


FIG. 3. A pictorial representation of the action of the plaquette operator \hat{U}_P .

$\lambda_s = 1$ (singlets). In the conventional $SU(2)$ LGT, the link representations λ_ℓ can take any irrep of $SU(2)$ from the set $\{\mathbf{1}$ (singlet), $\mathbf{2}$ (doublet), $\mathbf{3}$ (triplet), $\dots\}$. In contrast, qubit regularization restricts these to a finite subset. The simplest such scheme involves only $\lambda_\ell = \{\mathbf{1}, \mathbf{2}\}$ [12]. A natural question then arises: can we construct qubit-regularized $SU(2)$ LGTs within this minimal framework that exhibit nontrivial quantum critical points? Even more intriguing is the possibility of realizing massive continuum QFTs in the infrared by introducing relevant perturbations at these critical points. Recent studies have demonstrated that such behavior can indeed occur in qubit-regularized lattice spin models [13, 14]. Here, we show that analogous behavior emerges in the qubit-regularized $SU(2)$ plaquette chain.

The plaquette chain has the geometry of a ladder composed of two one-dimensional chains of lattice sites connected by rungs that link neighboring sites across the chains. We consider a system containing L plaquettes, which are connected periodically across the boundary. As stated, in the simplest $SU(2)$ qubit regularization discussed above, the Hilbert space on each link contains two types of dimer tensors, $\mathbf{0}$ and $\mathbf{2}$. A pictorial representation of an MDTN basis state for the plaquette chain is shown in Fig. 2.

The ladder geometry of the plaquette chain allows us to distinguish between two types of gauge links: those along the chains, which we label as ℓ_c , and those on the rungs connecting the two chains, labeled as ℓ_r . In addition, we define plaquettes P as the elementary squares formed by four such links. Using this notation, a generic gauge-invariant Hamiltonian for the plaquette chain can be written as

$$H = \kappa_c \sum_{\ell_c} \hat{\mathcal{E}}_{\ell_c} + \kappa_r \sum_{\ell_r} \hat{\mathcal{E}}_{\ell_r} - \delta \sum_P \hat{U}_P, \quad (2)$$

where the operator $\hat{\mathcal{E}}_\ell = (1 - \delta_{\lambda,1})$ is diagonal in the MDTN basis and assigns distinct energies to the different irreps on each link ℓ . In contrast, the plaquette operator \hat{U}_P is off-diagonal in the MDTN basis and flips all the irreps on the four links forming the plaquette, as illustrated in Fig. 3.

As explained in [11], in the absence of matter fields the $\mathbf{2}$ links form closed loops. These loops can either wind around the boundary or lie entirely within a finite region of the ladder. Consequently, the physical Hilbert space splits into a direct sum of two topologically distinct sectors, depending on the number of loops that cross the

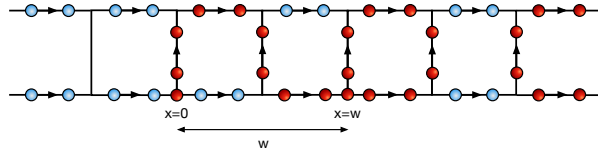


FIG. 4. A pictorial representation of an MDTN basis state of the $SU(2)$ plaquette chain with two heavy matter fields in the doublet representation located on the bottom rung at $x = 0$ and $x = w$.

boundary: $\mathcal{H}_{\text{phys}}^E$ (even sector, where zero or two loops cross the boundary) and $\mathcal{H}_{\text{phys}}^O$ (odd sector, where exactly one loop crosses the boundary). The Hamiltonian in Eq. (2) does not couple these two sectors. Moreover, the two Hilbert-space sectors can be distinguished locally by examining the link irreps on the top and bottom chains. Focusing on the two horizontal links of a given plaquette P , there are four possible basis states: $|\mathbf{11}\rangle$, $|\mathbf{12}\rangle$, $|\mathbf{21}\rangle$, and $|\mathbf{22}\rangle$, where the first label corresponds to the link irrep on the top chain and the second to that on the bottom chain. In $\mathcal{H}_{\text{phys}}^E$, each plaquette can be in either $|\mathbf{11}\rangle$ or $|\mathbf{22}\rangle$, while in $\mathcal{H}_{\text{phys}}^O$ it can be in either $|\mathbf{12}\rangle$ or $|\mathbf{21}\rangle$. Thus, the local plaquette Hilbert space \mathcal{H}_P spanned by the basis states $|\mathbf{11}\rangle$ and $|\mathbf{22}\rangle$ or $|\mathbf{12}\rangle$ and $|\mathbf{21}\rangle$ determines the full Hilbert space. The former belongs to the $\mathcal{H}_{\text{phys}}^E$ space and the latter belongs to the $\mathcal{H}_{\text{phys}}^O$ space.

The structure becomes richer when matter fields are introduced. The simplest case arises when two static matter fields in the doublet representation are placed at the bottom rungs of distinct lattice sites, say $x = 0$ and $x = w$. We view these as introducing heavy probe quarks in our pure gauge theory. In the presence of these heavy quarks, the local plaquette Hilbert space \mathcal{H}_P of the gauge theory changes from $\mathcal{H}_{\text{phys}}^E$ to $\mathcal{H}_{\text{phys}}^O$ (or vice versa) at the sites $x = 0$ and $x = w$, depending on the configuration of the surrounding links. We can now distinguish two further Hilbert-space sectors, $\mathcal{H}_{\text{phys}}^w$ and $\mathcal{H}_{\text{phys}}^{(L-w)}$. In the former, the plaquette Hilbert spaces between the sites $x = 0$ and $x = w$ belong to the $\mathcal{H}_{\text{phys}}^O$ sector, while in the latter they belong to the $\mathcal{H}_{\text{phys}}^E$ sector. An illustration of an MDTN basis state with two heavy matter fields in the $\mathcal{H}_{\text{phys}}^w$ sector is shown in Fig. 4.

When the sites $x = 0$ or $x = w$ contain four doublets (one from the heavy quark and three from the links connected to the site), there are two distinct ways to satisfy Gauss's law locally. This freedom is encoded in the index α_s in the MDTN basis. In this situation it is straightforward to verify that the action of \hat{U}_P on each of these two states produces the same unique state. Consequently, a particular linear combination of the two basis states is always annihilated by \hat{U}_P and therefore remains inert under the dynamics generated by Eq. (2). Operationally, it is as if the operator \hat{U}_P is effectively removed from the two adjacent plaquettes attached to the site $x = 0$ or $x = w$ whenever this special linear combination is chosen

in the MDTN basis.

Although one could in principle study the resulting effect of removing \hat{U}_P at the locations of the heavy matter fields, in this work we choose, for simplicity, to work with the orthogonal linear combination that is not annihilated by \hat{U}_P . This ensures that \hat{U}_P remains non-zero on all plaquettes, as in the original construction.

Introducing additional heavy quarks allows us to probe the rich gauge-theory Hilbert space more completely. Fixing the locations of the quarks defines new sectors of the theory, and the physics described by the Hamiltonian in each sector can differ in nontrivial ways. As we discuss below, within each such sector, the Hamiltonian in Eq. (2) can be mapped to a distinct TFIM.

III. MAPPING TO THE ISING MODEL

Let us first focus on the physics of H restricted to the even sector defined through the Hilbert space $\mathcal{H}_{\text{phys}}^E$. In this Hilbert space we can map the two possible plaquette states $|\mathbf{11}\rangle$ and $|\mathbf{22}\rangle$ to the quantum Ising Hilbert space of $|\uparrow\rangle$ and $|\downarrow\rangle$ respectively. This mapping is illustrated pictorially in Fig. 5. In this mapping the Hamiltonian of

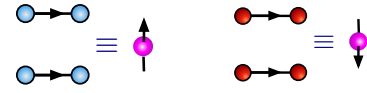


FIG. 5. Mapping the $|\mathbf{11}\rangle$ to $|\uparrow\rangle$ and $|\mathbf{22}\rangle$ to $|\downarrow\rangle$.

Eq. (2), in the $\mathcal{H}_{\text{phys}}^E$ sector, can be rewritten as

$$H^E = \sum_i \left(\kappa_c + \frac{\kappa_r}{2} - \frac{\kappa_r}{2} \sigma_i^z \sigma_{i+1}^z - \kappa_c \sigma_i^z - \delta \sigma_i^x \right), \quad (3)$$

where σ_i^z and σ_i^x are Pauli matrices associated to the plaquette P labeled by i . The states $|\uparrow\rangle$ and $|\downarrow\rangle$, illustrated in Fig. 5, are eigenstates of σ_i^z with eigenvalue +1 and -1 respectively. It is easy to see that the operator \hat{U}_P maps to σ_i^x . Similarly, the terms diagonal in this basis, along with the energies of the rung link are then given by terms in Fig. 6. These energies then allow us to Hamiltonian in

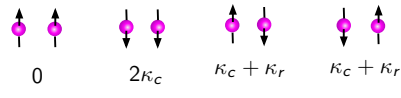


FIG. 6. Interaction energies of nearest neighbor spins. These energies are encoded in the diagonal matrix elements of Eq. (3).

Eq. (3).

We can repeat the above analysis to map the physics of H when restricted to the odd sector defined through the Hilbert space $\mathcal{H}_{\text{phys}}^O$. The final answer is can be rewritten as

$$H^O = \sum_i \left(\kappa_c + \frac{\kappa_r}{2} - \frac{\kappa_r}{2} \sigma_i^z \sigma_{i+1}^z - \delta \sigma_i^x \right), \quad (4)$$

κ_c	L	$\mathcal{E}_0(w=0)$	m_1	m_2	$\bar{\sigma}$	m_2/m_1	$\sqrt{\bar{\sigma}}/m_1$	$\kappa_c^{8/15}L$
0.3	12	-18.273(3)	2.834(3)	4.488(3)	0.2511(5)	1.584(3)	0.2497(10)	6.31
0.3	16	-24.363(3)	2.834(3)	4.548(3)	0.2507(3)	1.604(3)	0.2496(09)	8.42
0.2	16	-22.966(3)	2.287(3)	3.639(3)	0.1631(3)	1.591(3)	0.2494(10)	6.78
0.2	24	-34.448(2)	2.287(2)	3.679(2)	0.1628(1)	1.609(2)	0.2492(07)	10.17
0.1	28	-37.821(3)	1.583(3)	2.555(3)	0.0779(1)	1.614(5)	0.2490(11)	8.20
0.1	32	-43.224(3)	1.583(3)	2.555(3)	0.0779(1)	1.614(5)	0.2490(10)	9.37
0.1	48	-64.836(2)	1.584(2)	2.557(2)	0.0777(1)	1.614(3)	0.2486(9)	14.06
0.01	96	-122.8701(4)	0.4649(4)	0.7503(4)	0.00671(1)	1.614(2)	0.2489(9)	8.23

TABLE I. Using DMRG, we extract the ground-state energy of the lattice Hamiltonian Eq. (3) (after dropping the constant term) at $\kappa_r = 2$ and $\delta = 1$. This quantity is denoted by $\mathcal{E}_0(w=0)$. We also compute the two lowest glueball masses, m_1 and m_2 , as well as the string tension $\bar{\sigma}$, obtained from a linear fit to Eq. (7). The errors shown are determined from the fluctuations of the data points about the expected fit form, such that linear fits of the type shown in Fig. 7 have a $\chi^2/\text{d.o.f.}$ less than one. The string tension in units of energy-squared is given by $\sigma = \zeta \bar{\sigma}$ with $\zeta = 1.995(7)$ as explained in the text. The dimensionless ratios m_2/m_1 and $\sqrt{\bar{\sigma}}/m_1$ are expected to be universal quantities in the continuum gauge theory that depend on the scaling variable $\mu = \kappa_c^{8/15}L$, shown in the last column, in the limits $L \rightarrow \infty$ and $\kappa_c \rightarrow 0$. The E8QFT emerges when μ becomes large.

where σ_i^z and σ_i^x are Pauli matrices associated to the plaquette \mathcal{P} labeled by i as before, but now act on the $|\mathbf{12}\rangle$ and $|\mathbf{21}\rangle$ Hilbert space.

We can extend this analysis to include heavy quarks as discussed in the previous section. Such ‘static charges’ allow us to compute the static quark potential, from which we can compute the string tension σ in this linearly confining theory. In the next section we will argue that $\mathcal{H}_{\text{phys}}^E$ is a natural sector to explore the physics of plaquette chain. We can then compute the heavy quark potential by considering the ground state energies of the Hamiltonian of the theory in the Hilbert space sector $\mathcal{H}_{\text{phys}}^w$ as a function of w , assuming $w < L/2$. The Hamiltonian of the theory in this sector is then given by

$$H^w = \sum_i \left(\kappa_c + \frac{\kappa_r}{2} - \frac{\kappa_r}{2} \sigma_i^z \sigma_{i+1}^z - \kappa_c \theta_i \sigma_i^z - \delta \sigma_i^x \right), \quad (5)$$

where $\theta_i = 0$ for plaquettes between the sites $x = 0$ and $x = w$ and $\theta_i = 1$ outside. Comparing Eq. (5) and Eq. (3) we note that when $w = 0$, $H^w = H^E$.

IV. MASSIVE GLUEBALLS

In a confining theory, loops of **2**-links that wind around space are energetically suppressed, acquiring an energy proportional to the system size except at criticality. This observation suggests that the even sector, $\mathcal{H}_{\text{phys}}^E$, should be identified as the physical Hilbert space of local gauge-invariant excitations over the infinite-volume ground-state. In this sector, as argued in Section III, the Hamiltonian of the qubit-regularized SU(2) gauge theory on the plaquette chain can be mapped to Eq. (3), which becomes identical to Eq. (1) upon setting $\kappa_r = 2$, $\kappa_c = h$, and $\delta = 1$.

The physics of Eq. (1) has been extensively studied, and it is well known that for small nonzero values of h the

model flows to a massive QFT with hidden E_8 symmetry in the IR [4, 15, 16]. Zamolodchikov’s analysis predicts eight stable particles in the continuum QFT. However, except for the three lowest masses m_1 , m_2 , and m_3 , the higher masses lie above the two-particle thresholds of lighter states. These lightest three masses can be extracted from the four lowest energy levels, \mathcal{E}_i , $i = 0, 1, 2, 3$, of Eq. (1) at zero momentum using the relation $m_i = \mathcal{E}_i - \mathcal{E}_0$. In the limits $L \rightarrow \infty$ and $h \rightarrow 0$, these masses are expected to satisfy the analytic predictions [4],

$$\frac{m_2}{m_1} = 2 \cos \frac{\pi}{5} \approx 1.61803, \quad \frac{m_3}{m_1} = 2 \cos \frac{\pi}{30} \approx 1.98904, \quad (6)$$

which have been confirmed in several studies [17–19].

The above discussion can also be interpreted as being applicable to the qubit-regularized SU(2) gauge theory on the plaquette chain, restricted to the Hilbert space $\mathcal{H}_{\text{phys}}^E$ and defined by the Hamiltonian Eq. (2) with $\kappa_r = 2$, $\delta = 1$, and $\kappa_c \rightarrow 0$, describing a continuum QFT with massive particles that can be interpreted as pseudo-one-dimensional analogues of glueballs. The lowest three glueball masses satisfy the relations in Eq. (6).

We can also compute the static quark potential $V(w)$ between two heavy quarks as a function of their separation w by evaluating the ground-state energy $\mathcal{E}_0(w)$ of H^w , defined in Eq. (5). By fixing $\kappa_r = 2$ and $\delta = 1$, taking L to be sufficiently large, and choosing a variety of values of κ_c , confinement implies a functional dependence of the form

$$V(w) = \mathcal{E}_0(w) - \mathcal{E}_0(0) = \alpha + \bar{\sigma} w, \quad (7)$$

in the regime $1 \ll w \ll L$. The string tension $\bar{\sigma}$ is expected to depend strongly on κ_c but, once L is sufficiently large, should be independent of the system size. We have verified these expectations by computing $\mathcal{E}_0(w)$ using the DMRG method and display representative results

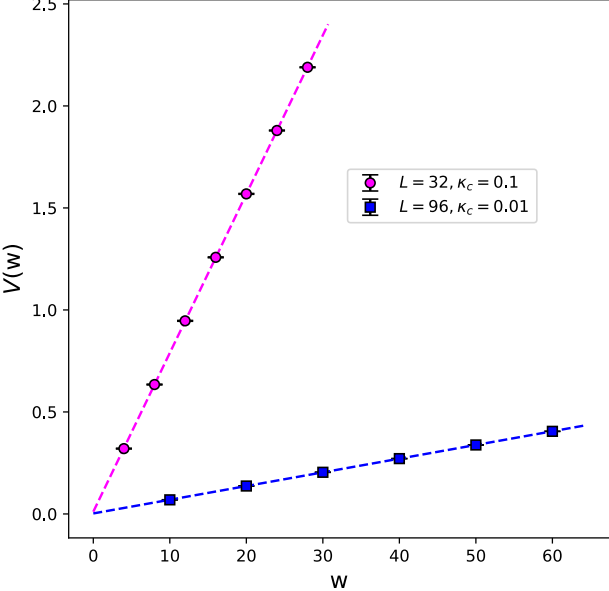


FIG. 7. Plot of the static quark potential $V(w)$ as a function of w at $(L = 32, \kappa_c = 0.1)$ and $(L = 96, \kappa_c = 0.01)$. These calculations were performed using DMRG. Because the uncertainties in the computed energies are difficult to estimate—and may be small enough that the data become sensitive to corrections beyond the linear form of Eq. (7)—we assigned errors of 0.002 to the $L = 32$ data and 0.0004 to the $L = 96$ data, consistent with the observed fluctuations about the fit; that is, these choices yield $\chi^2/d.o.f \sim 1$ for the linear fit.

for the heavy quark potential at $(L = 32, \kappa_c = 0.1)$ and $(L = 32, \kappa_c = 0.01)$ in Fig. 7.

The string tension $\bar{\sigma}$ has dimensions of energy per unit length. In a theory with explicit Lorentz invariance, one may work in natural units $\hbar c = 1$, in which case $\bar{\sigma}$ has the same dimensions as a mass squared. In a lattice Hamiltonian formulation, however, one must study the dispersion relation of the elementary excitations in order to extract an equivalent dimensionless quantity ζ . This allows us to define a physical string tension $\sigma = \zeta \bar{\sigma}$ with dimensions of energy squared, and hence to form the dimensionless ratio $\sqrt{\sigma}/m_1$, which is a universal quantity in the continuum QFT.

Because the lattice theory possesses discrete translational invariance, when the system is placed in a finite box of length L , each eigenstate of the Hamiltonian \mathcal{E}_i ($i = 0, 1, 2, \dots$) can be assigned a quantized momentum

$$p^{(n)} = \frac{2\pi n}{L}, \quad (8)$$

where the integer $n \in [-L/2, L/2]$. Energy eigenstates sharing the same momentum $p^{(n)}$ are labeled consecutively by an index $j = 0, 1, 2, \dots$, so that $\mathcal{E}_i \equiv \mathcal{E}_j^{(n)}$. The state with $j = 0$ and $n = 0$ is identified as the vacuum with energy \mathcal{E}_0 , while the higher $n = 0$ levels help define the masses m_j with $j = 1, 2, \dots$. Subtracting the vacuum

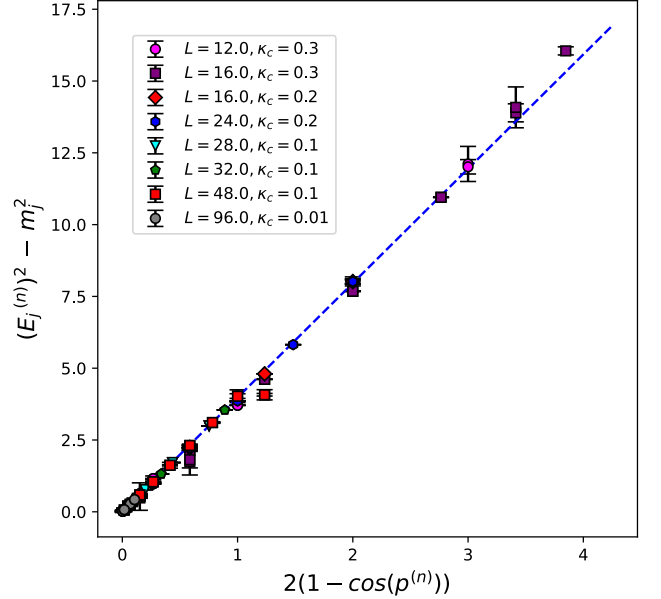


FIG. 8. Plot of the dispersion relation Eq. (10), demonstrating that all low-energy eigenvalues are consistent with a Lorentz-invariant form. The dashed line shows a linear fit to the $L = 96, \kappa_c = 0.01$ data; its slope is ζ^2 , yielding $\zeta = 1.995(7)$.

energy, we define the renormalized energies

$$E_j^{(n)} = \mathcal{E}_j^{(n)} - \mathcal{E}_0^{(0)}. \quad (9)$$

If the lattice theory describes a massive Lorentz-invariant QFT near the critical point, then at sufficiently large volumes the low-energy spectrum is expected to satisfy the dispersion relation

$$(E_j^{(n)})^2 = m_j^2 + \zeta^2 (p^{(n)})^2 + \mathcal{O}(n^4, L^{-4}), \quad (10)$$

where the parameter ζ is independent of both j and n . This same parameter was introduced above and serves to relate energy and length scales, playing the role of $\hbar c$ in the continuum dispersion relation.

We use DMRG to compute the low-lying energy spectrum for various values of L and κ_c , but we do not directly measure the momenta $p^{(n)}$. As a result, assigning the quantum numbers j and n to each energy level is nontrivial, particularly in the presence of numerical uncertainties. In our analysis, we first replace $(p^{(n)})^2$ in Eq. (10) by $2(1 - \cos p^{(n)})$, which is periodic over the Brillouin zone and coincides with the free-particle dispersion relation obtained from a naïve lattice discretization. We then label each nondegenerate state consecutively by an index j and identify its energy as m_j . For each fixed j , successive values of $|n|$ are assigned to pairs of degenerate states whenever their energies are consistent with the dispersion relation in Eq. (10). Degenerate states that do not satisfy this criterion are instead assigned to higher values of j and n , as appropriate.

Consistency is checked by fitting $(E_j^{(n)})^2$ as a function of $2(1 - \cos p^{(n)})$. For small values of the momentum, a linear fit is sufficient; however, due to the presence of lattice artifacts and, in some cases, the high accuracy of the data, higher-order terms in the dispersion relation become resolvable. In these cases, a polynomial fit upto third order is required to obtain an acceptable description. The resulting assignments of j and n to the various energy levels are summarized in [20]. To demonstrate that all low-energy levels are consistent with Eq. (10) with a single parameter ζ , we plot $(E_j^{(n)})^2 - m_j^2$ as a function of $2(1 - \cos p^{(n)})$ in Fig. 8. The dashed line in this figure corresponds to a linear fit to the $L = 96$, $\kappa_c = 0.01$ data, yielding $\zeta = 1.995(7)$.

Our DMRG analysis was performed using the ITensor software library in Julia [21, 22], and the fits were done using the NumPy [23] python package and the stats R package [24]. For the DMRG, we use cutoff parameters of 10^{-15} or smaller, perform 25 DMRG sweeps for each data point, and allow a maximum bond dimension of 400. Varying the bond dimension between 300 and 400 or the cutoff between 10^{-14} and 10^{-15} changes the results by less than 10^{-4} . Though this indicates that the DMRG calculations are well converged, the resulting points deviate from the expected linear behavior in Eq. (7) due to various residual errors including the w -dependence. These errors range from 0.002 for $L = 32$ to 0.0004 for $L = 96$ in the energy differences and are shown in Fig. 7. Our results for $\mathcal{E}_0(w)$, m_1 , m_2 , $\bar{\sigma}$ for several values of L and κ_c are listed in Table I. In this table, we also report the universal ratios m_2/m_1 and $\sqrt{\bar{\sigma}}/m_1$. While m_2/m_1 approaches the value predicted by E8QFT, we obtain the new universal dimensionless ratio $\sqrt{\bar{\sigma}}/m_1 = 0.249(1)$ in the continuum QFT.

V. ASYMPTOTIC FREEDOM

We can explore the physics of the massive continuum E8QFT in the uv. Since the critical lattice field theory flows to the IR fixed point governed by the ICFT, we expect the uv physics of the massive continuum E8QFT to be described by the same ICFT (see Fig. 1). If this expectation is correct, then, because the ICFT is known to be the theory of free massless Majorana fermions, we expect these Majorana fermions to be a manifestation of the bosonic scalar adjoint ‘gauge bosons’ attached to adjoint strings to project them onto the physical subspace of gauge-invariant states. We may then view the massive glueball states as arising through the confinement of these gauge bosons. In this interpretation, the $SU(2)$ gauge theory on the plaquette chain also exhibits the phenomenon of asymptotic freedom. The viewpoint that the massive states arise as bound states of free Majorana fermions is well known (see for example [25]).

Recently, it was discovered that asymptotic freedom and massive continuum QFT may arise from exotic RG

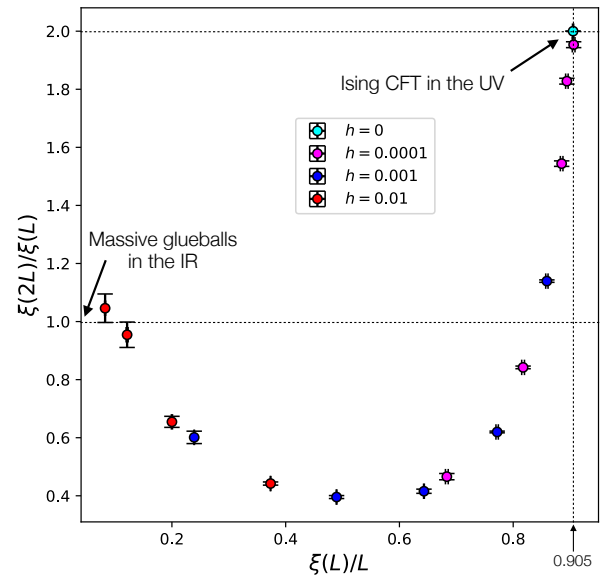


FIG. 9. Plot of the step-scaling function of the E8QFT using its mapping to the two-dimensional Ising model in a uniform magnetic field, whose Euclidean lattice action is given in Eq. (11). The correlation length $\xi(L)$ is extracted using Monte Carlo methods from the second-moment correlator of the subtracted field $(s_i - \bar{s})$, with \bar{s} defined as the spin expectation value in the magnetic field. In the UV, where we obtain the ICFT, we obtain the universal ratio $\xi(L)/L = 0.905(1)$. Our result is consistent with the known value $0.9050488292(4)$, obtained by numerically evaluating the exact CFT expressions for the torus two-point function and correlation-length amplitudes [26].

flows, in which the uv behavior is not governed by the IR fixed point of the critical qubit-regularized lattice field theory, but rather by a crossover fixed point that the RG trajectories approach before swinging away [13, 14]. To verify that no such exotic behavior occurs in the present case, using Monte Carlo methods, we have computed the step-scaling function of the E8QFT using the Euclidean lattice formulation of the Ising model defined by the action

$$S = -\beta_c \sum_{\langle ij \rangle} s_i s_j - h \sum_i s_i, \quad (11)$$

where $\beta_c = \log(1 + \sqrt{2})/2$ is the critical coupling at $h = 0$. At criticality Eq. (11) describes the same physics as Eq. (1) at long distances and low temperatures. The step-scaling function is defined in terms of the second-moment finite-size correlation length $\xi(L)$ [27], computed from correlation functions of the subtracted Ising field $(s_i - \bar{s})$ to account for the nonzero average magnetization \bar{s} when $h \neq 0$. The resulting step-scaling function is shown in Fig. 9.

VI. CONCLUSIONS

In this work, we have argued that the qubit-regularized $SU(2)$ lattice gauge theory (LGT) on a plaquette chain possesses a continuum limit in which it describes a non-trivial massive QFT. The massive excitations of this theory are one-dimensional analogs of glueballs, while in the UV the theory becomes asymptotically free and is described by free massless Majorana fermions. These features arise through an exact mapping of the LGT to the transverse-field Ising model (TFIM). Importantly, although the Hamiltonian of our qubit-regularized LGT differs from the conventional Kogut–Susskind Hamiltonian [28], it nevertheless retains the two essential ingredients of lattice gauge theories: an electric-field term that induces confinement and a magnetic-field term that promotes deconfinement. In our construction, the former appears as a diagonal operator that assigns different energies to different representations, while the latter enters through an off-diagonal plaquette operator.

It is natural to ask whether analogous features extend to $SU(3)$ LGTs. In this case, the qubit-regularized theory can be mapped to a class of three-state quantum clock models. Plaquette chains of this type have been explored recently in the context of Hamiltonian formulations and quantum computing [29, 30]. However, the study of critical points from which massive relativistic QFTs may emerge through the RG flow patterns illustrated in Fig. 1 remains largely unexplored. A straightforward $SU(3)$ extension of the qubit-regularized lattice gauge theory proposed here can be tuned to the relativistic critical point of the two-dimensional three-state Potts model [31]. Modifying the energies of the $SU(3)$ electric fields along the chain then introduces a uniform Potts’ magnetic field at criticality that favors one of the Potts states. This perturbation is relevant and can drive the theory to a massive relativistic QFT [32, 33]. We are currently exploring this massive QFT using DMRG.

Since qubit-regularized gauge theories are formulated within the Hamiltonian framework, they may realize both non-relativistic and relativistic quantum critical points [34,

35]. An important direction for future work is to engineer qubit-regularized gauge theories in higher dimensions that exhibit relativistic quantum critical points. Relevant deformations of these theories could then lead to massive relativistic continuum quantum field theories analogous to those constructed here.

ACKNOWLEDGMENTS

S.C. conceived of and carried out the initial investigations of this theory and created the outline of the manuscript. R.X.S. did the DMRG calculations. R.X.S. and S.C. did the Monte Carlo calculations, produced the figures, and produced the first draft of the paper. S.C. and T.B. provided the interpretation of the model in terms of a pseudo-one-dimensional gauge theory. All three authors refined the manuscript and agree with its final version.

S.C. would like to thank Ribhu Kaul and Hansen Wu for bringing the physics of the massive E_8 QFT to his attention. He also thanks Peter Orland and Berndt Müller for helpful conversations about the manuscript. We acknowledge the use of AI assistance, specifically ChatGPT [36] and Gemini [37], in searching the literature relevant to $SU(3)$ chains, refining the language and clarity of this manuscript, and providing citation to themselves, before our final rounds of manual review and revision by all authors. S.C. and R.X.S. are supported in part by the U.S. Department of Energy, Office of Science, Nuclear Physics program under Award No. DE-FG02-05ER41368. T.B. was supported by the U.S. Department of Energy, Office of Science, Office of High Energy Physics under contract number KA2401012 (LANL-E83G) at Los Alamos National Laboratory operated by Triad National Security, LLC, for the National Nuclear Security Administration of the U.S. Department of Energy (Contract No. 89233218CNA000001).

[1] S. Chandrasekharan, Qubit regularization of quantum field theories, *PoS LATTICE2024*, 001 (2025).

[2] C. W. Bauer, Z. Davoudi, N. Klco, and M. J. Savage, Quantum simulation of fundamental particles and forces, *Nature Rev. Phys.* **5**, 420 (2023), arXiv:2404.06298 [hep-ph].

[3] K. G. Wilson, The renormalization group and critical phenomena, *Rev. Mod. Phys.* **55**, 583 (1983).

[4] A. B. Zamolodchikov, Integrals of motion and S matrix of the (scaled) $T = T_c$ Ising model with magnetic field, *Int. J. Mod. Phys. A* **4**, 4235 (1989).

[5] P. Orland, Glueball masses in $(2 + 1)$ -dimensional anisotropic weakly-coupled Yang-Mills theory, *Phys. Rev. D* **75**, 101702 (2007).

[6] J. Nyhegn, C.-M. Chung, and M. Burrello, \mathbb{Z}_N lattice gauge theory in a ladder geometry, *Phys. Rev. Res.* **3**, 013133 (2021), arXiv:2011.06534 [quant-ph].

[7] S. Pradhan, A. Maroncelli, and E. Ercolessi, Discrete Abelian lattice gauge theories on a ladder and their dualities with quantum clock models, *Phys. Rev. B* **109**, 064410 (2024), arXiv:2208.04182 [hep-lat].

[8] X. Yao, $SU(2)$ gauge theory in $2 + 1$ dimensions on a plaquette chain obeys the eigenstate thermalization hypothesis, *Phys. Rev. D* **108**, L031504 (2023), arXiv:2303.14264 [hep-lat].

[9] L. Ebner, A. Schäfer, C. Seidl, B. Müller, and X. Yao, Entanglement entropy of $(2+1)$ -dimensional $SU(2)$ lattice gauge theory on plaquette chains, *Phys. Rev. D* **110**,

014505 (2024).

[10] F. Turro and X. Yao, Emergent hydrodynamic mode on SU(2) plaquette chains and quantum simulation, *Phys. Rev. D* **111**, 094502 (2025).

[11] S. Chandrasekharan, R. X. Siew, and T. Bhattacharya, Monomer-dimer tensor-network basis for qubit-regularized lattice gauge theories, *Phys. Rev. D* **111**, 114502 (2025), arXiv:2502.14175 [hep-lat].

[12] H. Liu and S. Chandrasekharan, Qubit regularization and qubit embedding algebras, *Symmetry* **14**, 305 (2022), arXiv:2112.02090 [hep-lat].

[13] T. Bhattacharya, A. J. Buser, S. Chandrasekharan, R. Gupta, and H. Singh, Qubit regularization of asymptotic freedom, *Phys. Rev. Lett.* **126**, 172001 (2021), arXiv:2012.02153 [hep-lat].

[14] S. Maiti, D. Banerjee, S. Chandrasekharan, and M. K. Marinkovic, Asymptotic freedom at the Berezinskii-Kosterlitz-Thouless transition without fine-tuning using a qubit regularization, *Phys. Rev. Lett.* **132**, 041601 (2024), arXiv:2307.06117 [hep-lat].

[15] G. Delfino and G. Mussardo, The spin-spin correlation function in the two-dimensional Ising model in a magnetic field at $T = T_c$, *Nucl. Phys. B* **455**, 724 (1995), arXiv:hep-th/9507010.

[16] G. Delfino and P. Simonetti, Correlation functions in the two-dimensional Ising model in a magnetic field at $T = T_c$, *Phys. Lett. B* **383**, 450 (1996), arXiv:hep-th/9605065.

[17] P. Fonseca and A. Zamolodchikov, Ising spectroscopy. I. mesons at $T < T_c$ (2006), arXiv:hep-th/0612304.

[18] R. G. Jha, A. Milsted, D. Neuenfeld, J. Preskill, and P. Vieira, Real-time scattering in Ising field theory using matrix product states, *Phys. Rev. Res.* **7**, 023266 (2025), arXiv:2411.13645 [hep-th].

[19] A. Karna, H. S. Wu, S. Chandrasekharan, and R. K. Kaul, Projected density matrix sampling for lattice Hamiltonians (2025), arXiv:2511.19209 [cond-mat.str-el].

[20] R. X. Siew, S. Chandrasekharan, and T. Bhattacharya, (2026), supplemental Materials for this article.

[21] M. Fishman, S. R. White, and E. M. Stoudenmire, The ITensor software library for tensor network calculations, *SciPost Phys. Codebases* **4** (2022).

[22] M. Fishman, S. R. White, and E. M. Stoudenmire, Codebase release 0.3 for ITensor, *SciPost Phys. Codebases* **4** (2022).

[23] C. R. Harris, K. J. Millman, S. J. van der Walt, R. Gommers, P. Virtanen, D. Cournapeau, E. Wieser, J. Taylor, S. Berg, N. J. Smith, R. Kern, M. Picus, S. Hoyer, M. H. van Kerkwijk, M. Brett, A. Haldane, J. F. del Río, M. Wiebe, P. Peterson, P. Gérard-Marchant, K. Sheppard, T. Reddy, W. Weckesser, H. Abbasi, C. Gohlke, and T. E. Oliphant, Array programming with NumPy, *Nature* **585**, 357 (2020).

[24] R Core Team, *R: A Language and Environment for Statistical Computing*, R Foundation for Statistical Computing, Vienna, Austria (2025).

[25] A. Litvinov, P. Meshcheriakov, and E. Shestopalov, Meson mass spectrum in Ising field theory, *Phys. Rev. D* **112**, 085021 (2025), arXiv:2507.15766 [hep-th].

[26] J. Salas and A. D. Sokal, Universal amplitude ratios in the critical two-dimensional Ising model on a torus, *J. Stat. Phys.* **98**, 551 (2000).

[27] S. Caracciolo, R. G. Edwards, A. Pelissetto, and A. D. Sokal, Asymptotic scaling in the two-dimensional O(3) σ model at correlation length 10^5 , *Phys. Rev. Lett.* **75**, 1891 (1995).

[28] J. B. Kogut and L. Susskind, Hamiltonian formulation of Wilson's lattice gauge theories, *Phys. Rev. D* **11**, 395 (1975).

[29] A. N. Ciavarella and I. A. Chernyshev, Preparation of the SU(3) lattice Yang-Mills vacuum with variational quantum methods, *Phys. Rev. D* **105**, 074504 (2022).

[30] A. N. Ciavarella and C. W. Bauer, Quantum simulation of SU(3) lattice Yang-Mills theory at leading order in large- N_c expansion, *Phys. Rev. Lett.* **133**, 111901 (2024).

[31] F. Y. Wu, The Potts model, *Rev. Mod. Phys.* **54**, 235 (1982).

[32] G. Delfino and P. Grinza, Confinement in the q -state Potts field theory, *Nucl. Phys. B* **791**, 265 (2008), arXiv:0706.1020 [hep-th].

[33] L. Lepori, G. Z. Toth, and G. Delfino, Particle spectrum of the 3-state Potts field theory: A numerical study, *J. Stat. Mech.* **0911**, P11007 (2009), arXiv:0909.2192 [hep-th].

[34] P. Orland and D. Rohrlich, Lattice gauge magnets: Local isospin from spin, *Nucl. Phys. B* **338**, 647 (1990).

[35] S. Whitsitt, R. Samajdar, and S. Sachdev, Quantum field theory for the chiral clock transition in one spatial dimension, *Phys. Rev. B* **98**, 205118 (2018).

[36] OpenAI, Chatgpt (gpt-4) (2025), accessed: 2025-02-14.

[37] Google, Gemini [Large Language Model] (2026), accessed: 2026-01-01.

SUPPLEMENTARY MATERIAL

Asymptotic-freedom and massive glueballs in a qubit-regularized $SU(2)$ gauge theory

Rui Xian Siew, Shailesh Chandrasekharan, and Tanmoy Bhattacharya

$\mathcal{E}_j^{(n)}/L$	$\delta\mathcal{E}_j^{(n)}/L$	j	n
$L = 16, \kappa_c = 0.3$			
-1.52271e+00	1.7e-05	0	0
-1.34561e+00	1.9e-06	1	0
-1.33964e+00	1.8e-06	1	1
-1.33964e+00	1.9e-06	1	1
-1.32336e+00	1.8e-06	1	2
-1.32336e+00	1.7e-06	1	2
-1.30048e+00	1.8e-06	1	3
-1.30048e+00	1.8e-06	1	3
-1.27500e+00	1.8e-06	1	4
-1.27500e+00	1.9e-06	1	4
-1.25042e+00	1.5e-06	1	5
-1.25042e+00	3.3e-05	1	5
-1.23849e+00	5.2e-05	2	0
-1.23519e+00	6.5e-05	2	1
-1.23487e+00	3.2e-03	2	1
-1.23008e+00	2.1e-03	1	6
-1.22881e+00	4.7e-03	1	6
-1.22671e+00	3.1e-03	2	2
-1.22628e+00	1.9e-03	2	2
-1.21602e+00	8.8e-04	1	7

$\mathcal{E}_j^{(n)}/L$	$\delta\mathcal{E}_j^{(n)}/L$	j	n
$L = 16, \kappa_c = 0.2$			
-1.43534e+00	1.2e-07	0	0
-1.29242e+00	8.8e-08	1	0
-1.28481e+00	4.9e-08	1	1
-1.28481e+00	3.9e-08	1	1
-1.26465e+00	1.1e-07	1	2
-1.26465e+00	2.1e-08	1	2
-1.23738e+00	5.2e-08	1	3
-1.23738e+00	4.5e-08	1	3
-1.20793e+00	4.4e-04	1	4
-1.20783e+00	1.4e-03	1	4
-1.20574e+00	7.8e-04	2	0
-1.20067e+00	3.1e-04	2	1

TABLE I. These tables show the assignment of the integers j and n to various energy levels. Note that the first two columns in each table give the energy density (not the energy) and its estimated error.

$\mathcal{E}_j^{(n)}/L$	$\delta\mathcal{E}_j^{(n)}/L$	j	n
$L = 24, \kappa_c = 0.2$			
-1.43534e+00	4.4e-08	0	0
-1.34006e+00	2.2e-06	1	0
-1.33776e+00	1.1e-06	1	1
-1.33776e+00	7.4e-08	1	1
-1.33127e+00	3.5e-07	1	2
-1.33127e+00	6.6e-07	1	2
-1.32155e+00	1.3e-07	1	3
-1.32155e+00	1.3e-07	1	3
-1.30973e+00	1.0e-07	1	4
-1.30973e+00	5.1e-08	1	4
-1.29684e+00	6.6e-08	1	5
-1.29684e+00	1.9e-07	1	5
-1.28203e+00	1.1e-03	2	0
-1.28370e+00	5.1e-04	1	6
-1.28370e+00	5.0e-04	1	6
-1.28065e+00	3.3e-04	2	1

$\mathcal{E}_j^{(n)}/L$	$\delta\mathcal{E}_j^{(n)}/L$	j	n
$L = 28, \kappa_c = 0.1$			
-1.35074e+00	1.6e-07	0	0
-1.29421e+00	2.9e-06	1	0
-1.29205e+00	1.3e-06	1	1
-1.29205e+00	3.0e-07	1	1
-1.28608e+00	7.7e-07	1	2
-1.28608e+00	1.4e-07	1	2
-1.27738e+00	7.4e-08	1	3
-1.27738e+00	1.1e-07	1	3
-1.26701e+00	1.2e-07	1	4
-1.26701e+00	1.2e-07	1	4
-1.25949e+00	2.3e-04	2	0
-1.25817e+00	7.8e-05	2	1
-1.25817e+00	1.0e-04	2	1

$\mathcal{E}_j^{(n)}/L$	$\delta\mathcal{E}_j^{(n)}/L$	j	n
$L = 32, \kappa_c = 0.1$			
-1.35074e+00	1.1e-07	0	0
-1.30128e+00	1.8e-05	1	0
-1.29983e+00	4.2e-06	1	1
-1.29983e+00	1.0e-05	1	1
-1.29574e+00	5.5e-06	1	2
-1.29574e+00	2.9e-06	1	2
-1.28962e+00	8.3e-07	1	3
-1.28962e+00	7.6e-08	1	3
-1.28214e+00	1.3e-07	1	4
-1.28214e+00	7.1e-07	1	4
-1.27386e+00	2.8e-05	1	5
-1.27386e+00	1.2e-05	1	5
-1.27089e+00	1.1e-04	2	0
-1.27002e+00	5.5e-05	2	1

TABLE II. These tables show the assignment of the integers j and n to various energy levels. Note that the first two columns in each table give the energy density (not the energy) and its estimated error.

$\mathcal{E}_j^{(n)}/L$	$\delta\mathcal{E}_j^{(n)}/L$	j	n
$L = 48, \kappa_c = 0.1$			
-1.35074e+00	9.5e-07	0	0
-1.31774e+00	2.3e-04	1	0
-1.31735e+00	2.2e-04	1	1
-1.31732e+00	4.6e-04	1	1
-1.31607e+00	1.9e-04	1	2
-1.31608e+00	2.4e-04	1	2
-1.31407e+00	5.0e-05	1	3
-1.31407e+00	1.3e-04	1	3
-1.31148e+00	4.2e-05	1	4
-1.31147e+00	3.8e-04	1	4
-1.30841e+00	1.1e-04	1	5
-1.30841e+00	5.2e-04	1	5
-1.30501e+00	8.0e-05	1	6
-1.30501e+00	2.3e-04	1	6
-1.30137e+00	3.5e-05	1	7
-1.30137e+00	1.2e-04	1	7
-1.29747e+00	3.3e-04	1	8
-1.29728e+00	1.8e-04	1	9
-1.29729e+00	7.2e-04	1	9
-1.29654e+00	9.6e-04	2	0
-1.29749e+00	9.1e-04	1	8
$L = 96, \kappa_c = 0.01$			
-1.27990e+00	4.5e-07	0	0
-1.27505e+00	1.1e-04	1	0
-1.27487e+00	4.3e-05	1	1
-1.27488e+00	1.0e-04	1	1
-1.27435e+00	3.3e-05	1	2
-1.27435e+00	3.2e-05	1	2
-1.27357e+00	1.3e-05	1	3
-1.27357e+00	5.1e-06	1	3
-1.27261e+00	1.5e-04	1	4
-1.27261e+00	1.8e-04	1	4
-1.27208e+00	3.2e-04	2	0
-1.27196e+00	1.9e-04	2	1
-1.27194e+00	3.1e-04	2	1
-1.27161e+00	1.7e-04	2	2
-1.27158e+00	3.4e-04	2	2
-1.27160e+00	2.2e-04	1	5
-1.27155e+00	3.5e-04	1	5
-1.27108e+00	2.4e-04	3	0

TABLE III. These tables show the assignment of the integers j and n to various energy levels. Note that the first two columns in each table give the energy density (not the energy) and its estimated error.